

- of *Dinosaurs*, K. Padian, Ed. (Cambridge Univ. Press, Cambridge, 1986), chap. 24; P. E. Olsen and H.-D. Sues, *ibid.*, chap. 25; J. F. Bonaparte, in *Actas II Cong. Arg. Pal. Bioestr.*, Buenos Aires, Argentina, 15 to 18 May 1978 (Universidad de Buenos Aires and Asociación Paleontológica Argentina, Buenos Aires, 1980), vol. 1, pp. 123–133.
15. J. F. Bonaparte, *Opera Lilloana* **22**, 1 (1971).
16. W. B. Harlan et al., *A Geological Time Scale* (Cambridge Univ. Press, Cambridge, 1989).
17. Etymology: *Palaeo*, early (Gk), and *chersis*, terrestrial turtle (Gk); *talampayensis*, after the provincial park of Talampaya, La Rioja, Argentina. We collected two specimens that are now housed at the Universidad Nacional de La Rioja. The type (UPVLR 68) is an articulated skeleton, complete except for the central part of the carapace. The specimen UPVLR 69 includes the endocranial cast, the right foot, and fragments of the carapace and plastron. Horizon and locality: Los Colorados Formation, Upper Triassic (Norian). Red siltstone with gypsum, 30 m below the top of the unit. Area between Quebrada de Los Jachaleros and La Esquina, about 6 km west of the 141 km marker, route 26, La Rioja province, Argentina. *Palaeochersis* is diagnosed by the following apomorphies: a quadratojugal that forms a large part of the cavum tympani; an angular with a strong ventral process; an anterior projection of the carapace beyond the margin of the plastron and overhanging most of the cervical vertebrae; an extensive transverse process of the ischium; a long hypischium underlying about five caudal vertebrae; and an extreme reduction or loss of the fifth-digit phalanges.
18. Putative sister groups to turtles are captorhinomorphs (4), procolophonids (5, 8), and pareiasaurids (6).
19. Characters are enunciated according to the derived condition unless otherwise stated. 1, External nares confluent; 2, external nares large and elongated; 3, narial platform; 4, lacrimal bone and duct absent; 5, orbital prominences and bosses absent; 6, unpaired vomer; 7, prefrontal-vomer contact; 8, squamosal-jugal contact absent; 9, palatal teeth on palatine and pterygoid (0), restricted to the medial portion of the pterygoids (1), absent (2); 10, vomerine teeth absent; 11, interpterygoid vacuity large and open (0), reduced (1), absent (2); 12, trochlear process absent (0), otic (1), pterygoid (2); 13, lateral vertical plate of pterygoid; 14, acute quadrate margin; 15, cavum tympani absent (0), moderately developed (1), deeply excavated (2); 16, opisthotic covered laterally by quadrate; 17, middle ear laterally walled; 18, sinus cavernosus; 19, facial nerve foramina separated from the sinus cavernosus; 20, vertical fenestra ovalis; 21, slender stapes; 22, quadrate pocket absent; 23, stapediotemporal canal anterior to fenestra ovalis; 24, basiptyergoid articulation fused; 25, basi-sphenoid-basioccipital? medial process unpaired (0), paired (1), absent (2); 26, recessus scalae tympani and perilymphatic fenestra defined by bone; 27, jugular posterior foramina defined by bone; 28, small anterior jugular foramina; 29, antrum postoticum; 30, supraoccipital crest; 31, wide transverse occipital plane with depressions for nuchal musculature; 32, temporal fossa roofed by overhanging process of skull roof; 33, temporal roof extended posterior to opisthotic; 34, processus paraoccipitalis of opisthotic tightly articulated to squamosal and quadrate; 35, supratemporal absent; 36, occipital condyle neck; 37, foramen magnum height greater than width; 38, small Meckelian fossa; 39, five vertebral scutes; 40, eleven peripheral bones; 41, supramarginal scutes absent; 42, marginals not separated by an anal notch; 43, plastron reaches posterior margin of ischium; 44, epiplastral hooks absent; 45, epiplastral processes articulating with carapace (0), present but without articulation (1), absent (2); 46, large prominent entoplastral keel absent; 47, articulation of cervical vertebrae concave or convex; 48, cervical ribs absent; 49, first dorsal rib smaller than second; 50, tenth dorsal vertebra fused to sacrum; 51, acromial process triangular plate (0), rodlike (1); 52, extensive subrectangular and platelike coracoid (0), absent (1); 53, coracoid foramina absent; 54, elongated iliac neck; 55, ventral ischial tubercle absent; 56, hypochium absent; 57, fused pelvis; 58, large anteromedial process of the ilium; 59, large thyroid fenestra on ischium and pubis; 60, phalangeal formula 2222?; and 61, posterior ischial shelf absent.
20. The matrix of Table 1 was examined with the programs PAUP [D. Swofford, *Phylogenetic Analysis Using Parsimony* version 3.1.1 (Smithsonian Institution, Washington, DC, 1993)] and Hennig86 (J. Farris, version 1.5, 1988). The analysis yielded a tree length of 77, a consistency index of 0.87, and a retention index of 0.89.
21. The large elongated nares are missing in the type but are shown by an additional skull, which is mostly unprepared and remains uncatalogued.
22. H. Bräm, *Schweiz. Palaeontol. Abh.* **83**, 1 (1965); M. S. Fernandez and M. S. de la Fuente, *Neues Jahrb. Geol. Palaeontol. Abh.* **193**, 81 (1994).
23. G. Cladera, G. W. Rougier, M. S. de la Fuente, A. B. Arcucci, in preparation.
24. Supported by grants to G.W.R. from the Sigma Xi Foundation, Asociación Amigos del Museo "Bernardino Rivadavia," CONICET (Argentina), and Deutsches Forschungsgemeinschaft (Germany). We thank E. Gaffney, F. de Broin, and J. Wible for extensive help and F. Abdala, G. Cladera, M. Isasi, D. Rougier, D. Pol, A. Forasiepi, S. Apesteguía, and S. Reuille for technical and field assistance.

24 January 1995; accepted 9 March 1995

Serpentine Stability to Mantle Depths and Subduction-Related Magmatism

Peter Ulmer and Volkmar Trommsdorff

Results of high-pressure experiments on samples of hydrated mantle rocks show that the serpentine mineral antigorite is stable to ~720°C at 2 gigapascals, to ~690°C at 3 gigapascals, and to ~620°C at 5 gigapascals. The breakdown of antigorite to forsterite plus enstatite under these conditions produces 13 percent H₂O by weight to depths of 150 to 200 kilometers in subduction zones. This H₂O is in an ideal position for ascent into the hotter, overlying mantle where it can cause partial melting in the source region for calc-alkaline magmas at a depth of 100 to 130 kilometers and a temperature of ~1300°C. The breakdown of antigorite in hydrated mantle produces an order of magnitude more H₂O than does the dehydration of altered oceanic crust.

It has been repeatedly proposed (1) that H₂O liberated from a subducted lithospheric slab may cause partial melting in the overlying mantle wedge, thus giving rise to subduction-related volcanism. Hydrothermal alteration of mantle rocks near the Earth's surface produces serpentine. Alteration is extensive in ocean basins (2) and along continental margins (3). Fully serpentinized peridotites (serpentinites) contain about 13% H₂O by weight; subduction of this altered mantle may thus transport large quantities of H₂O to depths of arc magma genesis, provided that serpentine minerals are stable to high pressures and temperatures. Serpentinites are thus potentially a more important source of H₂O than hydrated mafic oceanic crust, which contains <2% H₂O by weight at 3.0 GPa and 700°C (4). Through field evidence it has been demonstrated (5) that serpentine minerals are stable under eclogite facies conditions (2.0 GPa, 550°C). We describe here the results of an experimental study to evaluate the stability of serpentinite under these and higher pressure conditions.

Serpentinites [generalized formula Mg₃Si₂O₅(OH)₄] are trioctahedral phyllosilicates that have 1:1 octahedral-tetrahedral layer structures (6) and are composed of three basic minerals: chrysotile, lizardite, and an-

tigorite. Experimental studies (7) have demonstrated that antigorite is the only serpentine mineral stable at conditions up to 1.5 GPa and 650°C. In nature, antigorite forms either through breakdown of less stable serpentine minerals or directly from peridotite. Our experiments were therefore carried out on antigorite.

Antigorite [typical composition Mg_{2.82}-Si₂O₅(OH)_{3.64}] is composed of corrugated layers with a sinusoidal octahedral layer and a tetrahedral layer that reverses its polarity every half wavelength. The wavelength is variable and is expressed in terms of the number of tetrahedra (*m*) occurring along an entire wave. Some variations in composition and structure are common as a consequence of wavelike structural modulations (8). It is therefore crucial that in experimental investigations homogeneous material that is well characterized be used.

Such material cannot be obtained synthetically. We therefore chose a homogeneous natural antigorite [*m* = 17, ideal formula Mg₄₈Si₃₄O₈₅(OH)₆₂] that shows no structural or compositional modulations (9). This natural antigorite contains impurities (10). The calculated shift in the breakdown equilibrium curve of this antigorite with respect to a pure end-member, however, is in the range of experimental uncertainty (11). The sample separated from the rock (sample Mg159) consists of 85% antigorite and 15% brucite [Mg(OH)₂] by volume.

Institut für Mineralogie und Petrographie, Eidgenössische Technische Hochschule-Zentrum, CH-8092 Zürich, Switzerland.

The starting mixture was composed of 90% of the separate and 10% by weight of the high-temperature products [forsterite (Mg_2SiO_4) and enstatite ($MgSiO_3$)] obtained by reacting the original material at 1.0 GPa and 900°C for 48 hours in a piston-cylinder apparatus. This mixture is similar to that used by Evans *et al.* in their study of antigorite stability to a pressure P of 1.5 GPa (7). We included brucite, which reacts at low temperatures with antigorite to form forsterite + H_2O , to ensure that H_2O saturation was satisfied in the experiments, that is, $P_{H_2O} = P_{total}$. The amount of H_2O produced in this way is approximately 3.5% by weight.

We performed experiments at pressures up to 3.5 GPa on encapsulated samples in two piston-cylinder apparatuses. Runs lasted 100 to 250 hours (12). We carried out experiments at pressures from 3.5 to 8.0 GPa in a Walker-type multi-anvil apparatus on samples as described above with run durations of 12 to 50 hours (13).

After the runs had been completed by isobaric quenching, the capsules were pierced and inspected to assure the presence of H_2O . All recovered charges were analyzed by high-resolution x-ray diffraction, and a few by electron microprobe analysis. The direction of reaction was determined from shifts in the intensities of x-ray peaks. No shift in the positions of peaks was observed. Brucite was completely consumed in all run products. Olivine, which amounted to ~5% of the starting material, was, up to 6.6 GPa, always $\geq 15\%$ of the product assemblage, demonstrating that the low-temperature reaction of antigorite ($m = 17$) + 20 brucite \rightarrow 34 forsterite + 51 H_2O always went to completion.

Below 2.1 ± 0.2 GPa, antigorite reacted according to the reaction: antigorite ($m = 17$) \rightarrow 18 forsterite + 4 talc [$Mg_3Si_4O_{10}(OH)_2$] + 27 H_2O (Fig. 1). At higher pressures, antigorite reacted according to the reaction: antigorite ($m = 17$) \rightarrow 14 forsterite + 20 enstatite + 31 H_2O . Above 5.4 GPa the 10 Å phase [$Mg_3Si_4O_{10}(OH)_2 \cdot H_2O$] (14) was observed in addition. Above 6.6 GPa, the join forsterite- H_2O was no longer stable but was replaced by phase A [$Mg_7Si_2O_8(OH)_6$] plus enstatite. The breakdown of antigorite produced dense hydromagnesian phase A + enstatite. Where non-reacted antigorite was present in the charges, the 10 Å phase persisted to the highest pressures.

Earlier experiments involving serpentine above 5.0 GPa have indicated a considerably different pressure and temperature stability of the serpentine minerals (14-16). Experiments in synthetic ($MgO-SiO_2-H_2O$) systems and with natural antigorite resulted in a pressure stability of serpentine minerals of less than 5.5 GPa and less than

550°C at 5 GPa (14, 15); the breakdown products at 5 GPa were forsterite + 10 Å phase and phase A + 10 Å phase. In experiments on the breakdown of natural and synthetic antigorite (16), forsterite + enstatite was produced to 4.6 GPa (630°C) and clinoenstatite + brucite was produced at 5 GPa (500°C). All these experiments were performed with large amounts of ex-

cess H_2O in the starting mixes and with serpentines of unknown structural state.

Our data demonstrate a higher pressure-temperature (P - T) stability of antigorite than previously observed (14-16). We ascribe this discrepancy to two factors discussed below: (i) the influence of the structural state of the serpentine starting material; and (ii) occurrence of antigorite-free

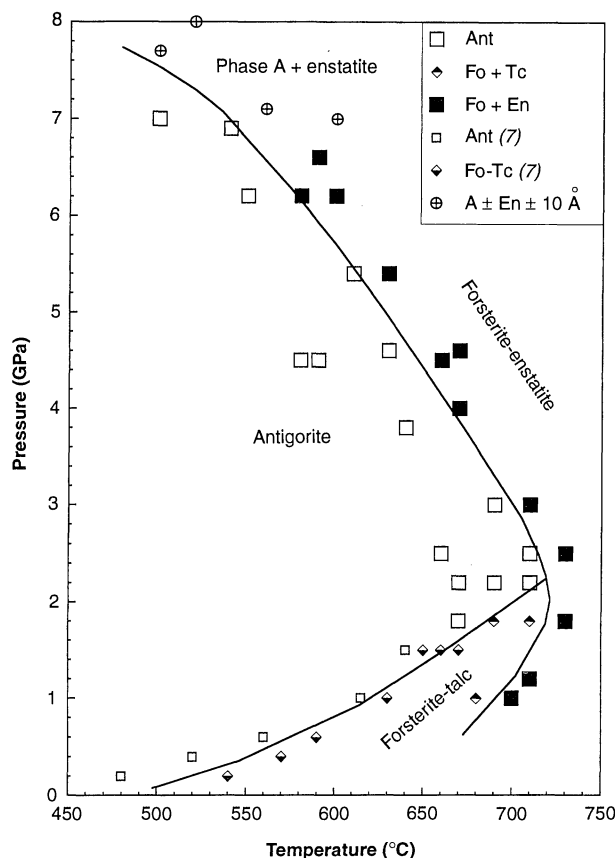
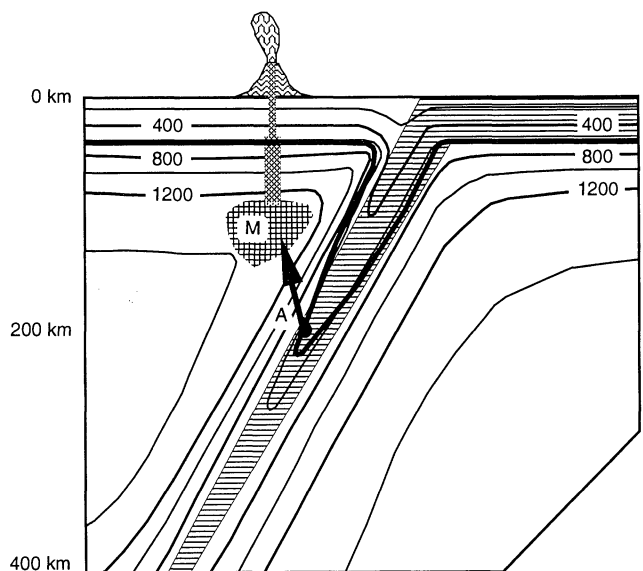


Fig. 1. Experimental pressure-temperature diagram for reactions involving the breakdown of antigorite and of forsterite + talc. Reaction curves are schematic and meet at an invariant point from which two additional curves (not shown) emanate. The invariant point lies at about 2.1 GPa and 730°C. Abbreviations are as in Table 1.

Fig. 2. Scenario for the subduction of oceanic lithosphere. Dip of subduction zone, 60°; velocity of subduction, 4.5 cm year⁻¹, temperatures in the mantle away from the slab, 1325°C, at a depth of 100 km [figure 5b in (18)]. The antigorite breakdown curve, corresponding to the reactions in Fig. 1, is shown by the thick curve. Antigorite enters the subducted lithospheric slab at a depth of ~200 km (point A). Antigorite breakdown would occur at greater depths in faster or steeper subduction zones and at shallower depth in shallower or slower subduction zones (19). Fluids produced at point A as a result of antigorite breakdown can reach the source region for calc-alkaline magma in the overriding mantle wedge (M) at a depth of 120 ± 35 km (7) as indicated by the arrow. The volcano is not to scale.



two-phase fields due to high silica solubility in the aqueous phase.

Most natural antigorite is characterized by imperfections, polysomatism, and structural disorder in addition to a variation in *m*. The contributions of the imperfections, which may approach over 20% by volume of the antigorite structure (9), to the configurational entropy of the mineral must be considerable.

The observed occurrence of the assemblage antigorite + phase A (runs 568 and 570, Table 1) requires metastability of the join forsterite + H₂O. At high silica solubility (17, 18), the three-phase field antigorite + phase A + fluid (relatively lower bulk H₂O) will be bounded by sizable two-phase fields; phase A + fluid [(14) relatively higher bulk H₂O] and antigorite + fluid (outside of our bulk composition). In order to determine the maximum stability of antigorite, the initial bulk H₂O contents of the charges must be carefully chosen.

Introduction of H₂O, released to the overlying mantle wedge in subduction

zones, is thought to trigger magmatism above the subduction zones (19). The release of H₂O has been considered a result of the breakdown of hydrous minerals in the subducting slab. Various minerals have been proposed as possible sources for H₂O release, including amphibole, chlorite, mica, lawsonite, and chloritoid (5, 20, 21). At ≥3 GPa and ≥600°C (19), mafic oceanic crust contains a maximum of 2% H₂O by weight, which is liberated episodically. In contrast, fully serpentinized peridotite contains 13% H₂O by weight, all of which could be liberated in a narrow *P-T* interval when the slab passes the antigorite breakdown condition above 2.1 GPa and below 6.6 GPa. Hydrated oceanic mantle is therefore about an order of magnitude more effective in producing H₂O at high pressures than mafic oceanic crust. In a "cold subduction environment," transport of H₂O to even greater depth is possible, if the geotherm passes a condition in which antigorite is replaced by assemblages containing the dense hydromagnesian phase A (21).

Serpentinite is abundant in oceanic basins and margins. Serpentinites with a thickness of 5 to 6 km have been identified through dredging, drilling, and seismic investigations in the Atlantic near the Galician margin (3). Serpentinite has been found in oceanic fracture zones (22), in seamounts of Pacific forearc regions (23, 24), and also in several areas away from continental margins and transform zones (2). Hydrated mantle consists of more than 90% serpentine minerals. It is very likely that large volumes of serpentinite, especially serpentinized ocean floor, are subducted together with other oceanic lithosphere in subduction zones.

So far, amphibole generally has been regarded to be the most effective H₂O source for subduction-related volcanism (19). Its stability is, however, limited to pressures of 2.3 GPa in basaltic compositions (25) and to 3.0 GPa in peridotitic compositions (26). This restriction has led to complicated models for H₂O transport to the source regions of calc-alkaline volcanism (19). Because antigorite is stable to 7.0 GPa, H₂O from the breakdown of antigorite in subduction zones can be released below the source region of arc-type volcanism. During ascent, this H₂O cannot be consumed by the crystallization of amphibole because the ascent in the subducted slab and mantle wedge (arrow in Fig. 2) follows a *P-T* trajectory in which amphibole is not stable. Our results suggest that the dominant mechanism for H₂O transport to great depths is the subduction of hydrated oceanic mantle.

Table 1. Data for the antigorite experiments. Starting material: FT/E, reversed experiments using (i) synthetic forsterite + talc + H₂O and (ii) synthetic enstatite + H₂O; AB, 85% antigorite Mg₁₅₉c (9) and 15% brucite; ABFE, 90% AB and 10% product (forsterite plus enstatite produced at 1.6 GPa, 850°C). Product phases: A, phase A [Mg₇Si₂O₅(OH)₆]; Ant, antigorite; Chl, chlorite; En, enstatite; Fo, forsterite; Tc, talc; 10 Å, 10 Å phase [Mg₃Si₄O₁₀(OH)₂·H₂O]; minus sign, amount of phase decreased; and parentheses, phase present only in trace amounts. Technique: MA, Walker-type multi-anvil device; BE, end-loaded piston cylinder; and JO, non-end-loaded piston cylinder.

Run number	<i>P</i> (GPa)	<i>T</i> (°C)	Starting material	Time (hours)	Technique	Product phases
r4	1.0	680	FT/E	70.0	JO	Fo, Tc
r1	1.0	700	FT/E	72.0	JO	En
528	1.2	710	ABFE	139.0	JO	Fo, En
515	1.8	670	ABFE	257.1	JO	Ant, Fo
517	1.8	690	ABFE	100.0	JO	Fo, Tc, -En, -Ant
522	1.8	710	ABFE	70.2	BE	Fo, Tc, -Ant
523	1.8	730	ABFE	69.2	JO	Fo, En, Chl
516	2.2	670	AB	236.6	BE	Ant, Fo
520	2.2	690	ABFE	65.7	BE	Ant, Fo
526	2.2	710	ABFE	70.4	BE	Ant, Fo, En
508	2.5	660	AB	70.0	BE	Ant, Fo
527	2.5	710	ABFE	63.6	BE	Ant, Fo
544	2.5	730	ABFE	70.6	BE	Fo, En, -Ant
545	3.0	710	ABFE	71.0	BE	Fo, En, -Ant
546	3.0	690	ABFE	68.1	BE	Ant, Fo
551	3.8	640	ABFE	26.2	MA	Ant, Fo
550	4.0	670	ABFE	40.8	MA	Fo, En, Chl, -Ant
509	4.5	580	AB	6.6	MA	Ant, Fo
511	4.5	620	AB	6.0	MA	Ant, Fo, (En)
507	4.5	660	AB	5.5	MA	Fo, En
553	4.6	630	ABFE	22.3	MA	Ant, Fo
549	4.6	670	ABFE	40.0	MA	Fo, En, Chl, -Ant
554	5.4	610	ABFE	30.0	MA	Ant, Fo
555	5.4	630	ABFE	30.0	MA	Fo, En, (Chl), -Ant
513	6.2	550	AB	5.5	MA	Ant, Fo, 10 Å
514	6.2	590	AB	6.5	MA	Fo, 10 Å, -Ant
565	6.2	600	ABFE	11.0	MA	Fo, En, -Ant
569	6.6	580	ABFE	23.8	MA	Fo, En, 10 Å, -Ant
570	6.9	540	ABFE	28.0	MA	Ant, A, 10 Å
568	7.0	500	ABFE	20.0	MA	Ant, A, 10 Å
566	7.0	600	ABFE	12.2	MA	A, En
571	7.1	560	ABFE	30.0	MA	A, En, 10 Å, -Ant
519	7.7	500	ABFE	8.0	MA	A, En
567	8.0	520	ABFE	11.0	MA	A, (En), (10 Å)

REFERENCES AND NOTES

- A. R. Pawley and J. R. Holloway, *Science* **260**, 664 (1993).
- Th. Juteau, M. Canniat, Y. Lagabrielle, *Proc. Ocean Drill. Program Sci. Results* **106-109**, 303 (1990).
- G. Boillot, J. Girardeau, J. Kornprobst, *ibid.* **103**, 741 (1988).
- J. Gill, *Orogenic Andesites and Plate Tectonics* (Springer-Verlag, New York, 1981).
- M. Scambelluri, O. Müntener, J. Hermann, G. B. Piccardo, V. Trommsdorff, *Geology*, in press.
- F. J. Wicks and D. S. O'Hanley, *Rev. Mineral.* **19**, 91 (1988).
- B. W. Evans, W. Johannes, H. Oterdoorn, V. Trommsdorff, *Schweiz. Mineral. Petrogr. Mitt.* **56**, 79 (1976).
- G. Kunze, *Fortschr. Mineral.* **39**, 206 (1961). The reversals in the polarity of the tetrahedral layers are of two alternating kinds: at one type of reversal, three Mg(OH)₂ units are missing; at the other one, none. The wavelength of antigorite, expressed as the number of tetrahedra (*m*) along an entire wavelength, has been observed to vary at least between *m* = 13 and *m* = 40, corresponding to 32.6 Å and 100 Å, respectively. Accordingly, antigorite forms a series of discrete compositions, each corresponding to a wavelength *m*, making up a polysomatic series. This series can be expressed by the general formula 1/*m*[Mg_{3*m*-3}Si_{2*m*}(OH)_{4*m*-6}]. A typical composition with *m* = 17 is Mg_{2.82}Si₂O₅(OH)_{3.64}. Antigorites with high *m* are compositionally closer to chrysotile, Mg₃Si₂O₅(OH)₂; those with low *m* are closer to talc, Mg₃Si₄O₁₀(OH)₂.
- M. Mellini, V. Trommsdorff, R. Compagnoni, *Contrib. Mineral. Petrol.* **97**, 147 (1987).

10. The chemical composition of antigorite from rock sample Mg159c (in percent by weight) is: SiO₂, 43.32; Cr₂O₃, 0.23; Al₂O₃, 1.30; Fe₂O₃, 0.50; FeO, 2.59; MnO, 0.04; MgO, 39.62; NiO, 0.08. The x_{Mg} (= molar MgO/(MgO+FeO)) = 0.965; $x_{Fe^{3+}}$ (= molar Fe³⁺/Fe_{tot}) = 0.15 (determined by Mössbauer spectroscopy).
11. V. Trommsdorff and B. W. Evans, *Am. J. Sci.* **272**, 423 (1972).
12. Up to 2.2 GPa we used a non-end-loaded piston cylinder with a 19-mm bore. From 2.2 to 3.5 GPa we used an end-loaded piston cylinder with 14-mm bore. We encapsulated 15 to 20 mg of the starting mix in Ag₅₀Pd₅₀ containers and welded them shut; NaCl assemblies were used. Pressures are considered to be accurate to within ± 0.05 GPa. Temperatures were measured with shielded Chromel-Alumel (Phillips) thermocouples (up to 2.2 GPa) and Pt-Pt₁₀Rh thermocouples at higher pressures. Temperatures were controlled to within ± 2°C but not corrected for pressure.
13. D. Walker, M. A. Carpenter, C. M. Hitch, *Am. Mineral.* **75**, 102 (1990); D. Walker, *ibid.* **76**, 1092 (1991). Multi-anvil experiments (up to 2.2 GPa) were performed with tungsten carbide cubes with a truncated edge length of 12 mm. The pressure-transmitting octahedron and gasket fins were fabricated from MgO-based castable ceramics (Ceramacast 584) and fired at 1150°C for at least 6 hours. Stepped graphite furnaces of 3.5 mm outside diameter and 3.1 mm inside diameter (2.7 mm central stepped area) were used to minimize temperature gradients. Approximately 3 to 4 mg of starting material were placed in 1.6-mm Ag₅₀Pd₅₀ or Pt capsules that were then welded shut. Temperatures were measured with two Pt-Pt₁₀Rh thermocouples inserted laterally from the fins. Measured temperature gradients at 600°C were less than 10°C/mm. Temperatures of the multi-anvil experiments (Table 1) were not corrected for pressure and are considered to be accurate to within ± 10°C. Pressure was calibrated at room temperature against the phase transitions in Bi metal and at high temperature (1000° to 1200°C) against the transformations of quartz to coesite (1200°C, 3.2 GPa) [S. R. Bohlen and A. L. Boettcher, *J. Geophys. Res.* **87**, 7073 (1982)], coesite to stishovite (1000°C, 9.1 GPa) [T. Yagi and S.-I. Akimoto, *Tectonophysics* **35**, 259 (1976)], fayalite (Fe₂SiO₄) to γ -spinel (1000°C, 5.0 GPa) [T. Yagi, M. Akaogi, O. Shimomura, T. Suzuki, S.-I. Akimoto, *J. Geophys. Res.* **92**, 6207 (1987)], and the phase transformation of CaGeO₃ from garnet to perovskite structures (1000°C, 6.1 GPa) [J.-I. Susaki, M. Akaogi, S.-I. Akimoto, O. Shimomura, *Geophys. Res. Lett.* **12**, 729 (1985)]. Pressures are considered to be accurate to within ± 0.2 GPa between 3.5 and 8 GPa. We quenched the piston cylinder and multi-anvil experiments isobarically by turning off the heating power; quenching rates for both types of apparatus were in the range 300° to 500°C per second.
14. K. Yamamoto and S.-I. Akimoto, *Am. J. Sci.* **277**, 288 (1979).
15. O. Yu. Khodyrev and M. Agoshkov, *Geochem. Int.* **23** (no. 7), 47 (1986).
16. B. Wunder and W. Schreyer, *Ber. Deutsch. Min. Ges. Beih. Eur. J. Min.* **6** (no. 1), 316 (1994).
17. C. E. Manning, *Mineral. Mag. A* **58**, 5515 (1994).
18. I. D. Ryabchikov, W. Schreyer, K. Abraham, *Contrib. Mineral. Petrol.* **79**, 80 (1982).
19. J. H. Davies and D. J. Stevenson, *J. Geophys. Res.* **97**, 2037 (1992).
20. M. W. Schmidt and S. Poli, *Earth. Planet. Sci. Lett.* **124**, 105 (1994).
21. A. B. Thompson, *Nature* **358**, 295 (1992).
22. E. Bonatti and K. Crane, *Sci. Am.* **250**, 36 (May 1984).
23. P. Fryer, E. L. Ambos, D. M. Hussong, *Geology* **13**, 774 (1985).
24. M. J. Keen and M. Salisbury, *Geosci. Can.* **16**, 177 (1990).
25. R. E. T. Hill and A. L. Boettcher, *Science* **167**, 980 (1970).
26. D. H. Green, *Earth Planet. Sci. Lett.* **19**, 37 (1973).
27. We acknowledge the constructive reviews of J. A. D. Connolly, B. W. Evans, R. J. Sweeney, D. Bernoulli, B. Wunder, and M. Mellini as well as the comments of two anonymous reviewers. This work was supported under Swiss National Science Foundation grant 2000-037388.93/1.

20 December 1994; accepted 9 March 1995

Dinitrogen Cleavage by a Three-Coordinate Molybdenum(III) Complex

Catalina E. Laplaza and Christopher C. Cummins*

Cleavage of the relatively inert dinitrogen (N₂) molecule, with its extremely strong N≡N triple bond, has represented a major challenge to the development of N₂ chemistry. This report describes the reductive cleavage of N₂ to two nitrido (N³⁻) ligands in its reaction with Mo(NR₂)₃, where R is C(CD₃)₂CH₃ and Ar is 3,5-C₆H₃(CH₃)₂, a synthetic three-coordinate molybdenum(III) complex of known structure. The formation of an intermediate complex was observed spectroscopically, and its conversion (with N≡N bond cleavage) to the nitrido molybdenum(VI) product N≡Mo(NR₂)₃ followed first-order kinetics at 30°C. It is proposed that the cleavage reaction proceeds by way of an intermediate complex in which N₂ bridges two molybdenum centers.

The relatively inert dinitrogen molecule (N₂) composes 78% of the Earth's atmosphere; the development of this molecule's chemistry is clearly desirable if this immense natural resource is to be utilized optimally. In this regard, the discovery of mild methods for scission of the N≡N triple bond represents a major challenge. Although the metalloenzyme nitrogenase constitutes a unique biological nitrogen-fixing system (1) and the Haber-Bosch ammonia synthesis is an example of industrial nitrogen fixation (2), little molecular-level detail is available concerning the critical N₂ cleavage processes operative for either of these processes. Well-characterized synthetic systems capable of splitting N₂ have been elusive (3), despite the mul-

titude of known transition-metal complexes containing intact dinitrogen as a ligand (4). In connection with a study on cleavage of the N–N bond in nitrous oxide (N₂O), Laplaza *et al.* reported (5) the synthesis and structural characterization of the three-coordinate Mo(III) complex Mo(NR₂)₃ [1, where R = C(CD₃)₂CH₃ and Ar = 3,5-C₆H₃Me₂ (Me, methyl), Fig. 1]. We now report the reductive scission of N₂ to two N³⁻ ligands in its reaction with 1. The reaction occurs in hydrocarbon solution at low temperatures (–35° to 30°C) and pressures (1 atm).

Purification of red-orange 1 consisted of recrystallization under an Ar atmosphere (ethyl ether, 0.1 M, –35°C). When we attempted to purify 1 by recrystallization under an atmosphere of N₂, the solutions (ethyl ether, 0.1 M, –35°C) took on an intense purple color in less than 45 min. Examination of the purple

solutions by ²H nuclear magnetic resonance (NMR) spectroscopy (6) revealed that the signal at 64 parts per million (ppm) for 1 was being replaced by a single new peak at 14 ppm, attributable to the purple species (2, Fig. 2). When we carried out the reaction using pure 1 in toluene (leaving all other conditions unchanged), from which the complex crystallizes less readily, complete conversion to 2 took approximately 48 hours at –35°C. On warming to 30°C, the purple solutions of 2 gradually became gold and lost their paramagnetism. Removal of all volatile material in vacuo left an amber crystalline residue that dissolved readily in benzene-*d*₆ for ¹H NMR spectroscopic analysis. The ¹H NMR spectroscopy showed that a terminal nitrido Mo(VI) complex (3, Fig. 2), identical to the complex that we isolated

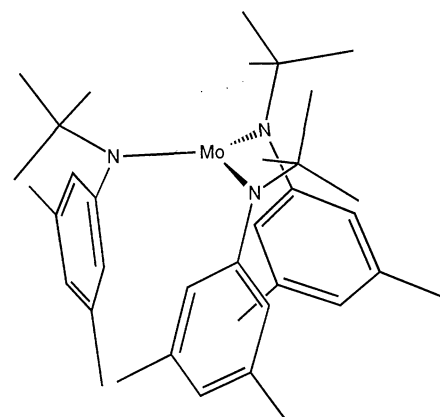


Fig. 1. Line drawing of the molecular structure of Mo(NR₂)₃ (1). The structure of 1 was determined by x-ray crystallography (5).

Department of Chemistry, Massachusetts Institute of Technology, Cambridge, MA 02139, USA.

*To whom correspondence should be addressed.